Mon. Not. R. Astron. Soc. **000**, 1–?? (2009) Printed 1 November 2009 (MN LaTeX style file v2.2)

On the nulls, modes and interpulse emission of radio pulsar B1944+17

Isabel M. Kloumann[1] & Joanna M. Rankin[2,1]
[1] *Physics Department, University of Vermont, Burlington, VT 05405*⋆
[2] *Sterrenkundig Instituut 'Anton Pannekoek', University of Amsterdam, NL-1098 XH*

Accepted 2009 month day. Received 2009 month day; in original form 2009 month day

ABSTRACT
We present a single pulse study of pulsar B1944+17, whose non-random nulls dominate nearly 70% of its pulses and usually occur at mode boundaries. Geometric modeling indicates that this pulsar is a nearly aligned rotator whose α value is some 6°—*i.e.*, its magnetic axis is closely aligned with the rotation axis. B1944+17 displays a weak interpulse whose position relative to the main pulse ($\Delta\phi_{IP-MP}$) we find to be frequency independent. Its emission is nearly 100% polarized, that its polarization-angle traverse is equal in magnitude and opposite in direction to that of the main pulse, and it is in the null state approximately two-thirds of the time (just as the main pulse is). The near alignment of the axes combined with its highly polarized interpulse suggest they reflect an unusual emission geometry. When not in the null state, this pulsar displays four bright modes of emission, three of which exhibit drifting subpulses. The interpulse's weak intensity prevents us from investigating its subpulse structure for comparison with that of the main pulse.

Key words: miscellaneous –null– interpulse – emission modes – methods: — data analysis – pulsars: general, individual (B1944+17)

1 INTRODUCTION

Pulsar B1944+17 was discovered in August 1969 at the Molonglo Radio Observatory. This 440-ms pulsar attracted attention thereafter because of its long null intervals. Remarkably, it nulls some 70% of the time and exhibits null lengths ranging in duration between 1 and 300 stellar-rotation periods (hereafter P_1). In 1986 Deich *et al.* (hereafter DCHR) investigated B1944+17's nulling behavior based on the received notion that its nulls represented "turn offs" of the pulsar emission mechanism. Thus they were concerned with the time scales of the cessations and resumptions of emission. While some pulsars, indeed, do appear to "turn off" for extended intervals—notably B1931+24 (Kramer *et al.* 2006)—there is a growing body of evidence that many nulls do not represent a shutdown of a pulsar's emission engine.

Specifically, we now know that conal beams are comprised of rotating "carousels" of subbeams, and in certain situations nulls (or what might better be called *pseudo*nulls) represent "empty" sightline passes through a subbeam carousel. Such carousel "action" was first demonstrated in pulsar B0943+10 (*e.g.*, Deshpande & Rankin 1999, 2001; Suleymanova & Rankin 2009), and then *pseudo*nulling was identified in pulsars B2303+30 (Redman *et al.* 2005; B0834+06 (Rankin & Wright 2007) and J1819+1305 (Rankin & Wright 2008). Furthermore, periodicites clearly associated with nulling were discovered in pulsar B1133+16 by Herfindal & Rankin (2007) and then subsequently in a number of other stars (Herfindal & Rankin 2009; hereafter HR07/09), and such periodicities are almost certainly carousel related.

There remain a small number of pulsars, however—B1944+17 prominent among them—whose observed nulling effects are not easily ascribed to either mechanism. That is, neither emission cessations, marked by partial nulls or measurable decay times, nor "empty" sightline traverses through a rotating subbeam carousel, marked by null periodicites, provide any clear explanation.

Pulsar B1944+17 exhibits a complex combination of behaviors including two distinct null behaviors: short nulls (1-15 P_1), and long nulls (> 15 P_1). In addition, DCHR identified what appeared to be several distinct emission modes, denoted A-D. And furthermore, Hankins & Fowler (1986; hereafter HF86) discovered that B1944+17 has a weak interpulse that nulls in synchrony with its main-pulse region (hereafter IP/MP). Synchronous nulling indicates, remarkably, that whatever mechanism is responsible for MP nulling is also controlling the IP emission.

⋆ Isabel.Kloumann@uvm.edu; Joanna.Rankin@uvm.edu

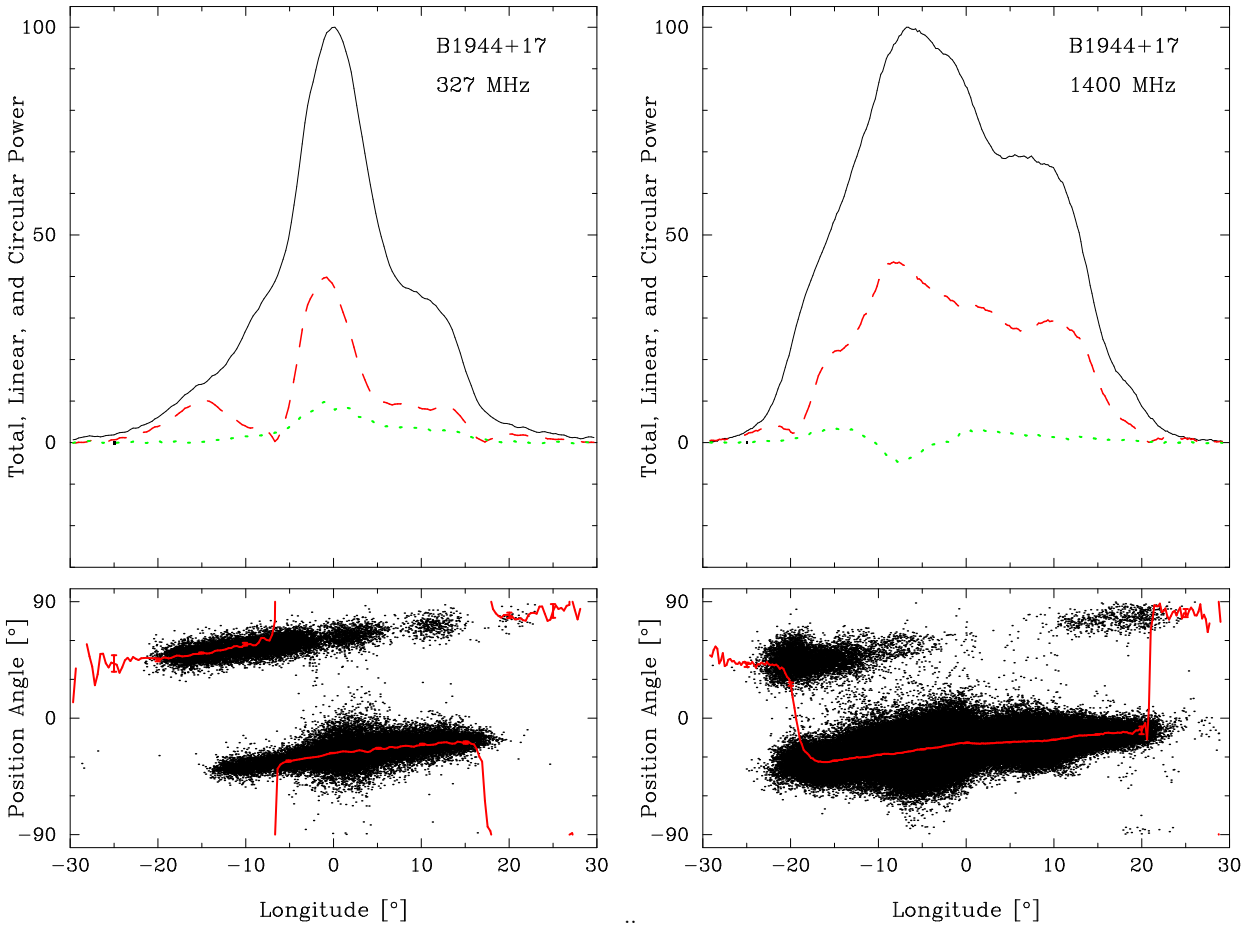

(a) 327-MHz PPA histogram comprised of 7038 pulses

(b) 1400-MHz PPA histogram comprised of 5470 pulses

Figure 1. The two panels display the total power (Stokes I), total linear polarization (L $[=\sqrt{Q^2+U^2}]$; dashed red) and circular polarization (Stokes V, defined as left-hand – right-hand circular polarization; dotted green) (upper), and the polarization angle (PPA $[=\frac{1}{2}\tan^{-1}(U/Q)]$) (lower). Individual samples that exceed an appropriate >2 sigma threshold appear as dots with the average PPA (red curve) overplotted. The small box at the left of the upper panel gives the resolution and a deflection corresponding to three off-pulse noise standard deviations. The PPAs are approximately absolute, such that the discontinuous regions of OPM emission at positive and negative PPAs correspond to each other. Note that the P and L band profiles each extend to about ±20° and that the lower frequency profile has an unusually narrow equivalent width relative to its higher frequency counterpart.

The fact of both MP and IP emission raises vexing questions about the overall emission geometry of the star. Several analyses of pulsar geometry (*e.g.*, Lyne & Manchester 1988; Rankin 1993, hereafter R93) have mentioned B1944+17, but as for virtually all such pulsars, no credible model of its overall MP-IP emission geometry has yet been articulated. In short, neither an "opposite pole" nor "single pole" IP geometry provides a reasonable solution, so among the various other issues, this basic question is still open for B1944+17.

When not in the null state MP pulse sequences (hereafter PSs) exhibit four fairly distinct modes of emission, three of which are well defined drift modes. The burst lengths last for up to 100 pulses, indicating a non-random null-burst distribution. The strict organization of the principle drift mode (Mode A, to be defined below) is in stark contrast with the disorganized non-drifting burst mode (Mode D) as well as the pulsar's preponderance of null pulses.

The rich variety of phenomena exhibited by this pulsar complicates its analysis, as well as any effort at modeling its many phenomena. While B1944+17 exhibits so many different identifiable behaviors (organized drifting, nearly "chaotic" subpulse behavior, bright emission, short nulls, long nulls, etc.), what makes the star so compelling is that in any time interval of reasonable length, (∼2000 P_1), one *will* see each of these behaviors. This consistency indicates that the processes that produce such variable emission patterns are in some way repeating themselves.

This paper reports a new synthetic study of pulsar B1944+17. We have conducted long, high quality polarimetric observations using the upgraded Arecibo telescope at both meter and decimeter wavelengths, carefully analyzed the star's emission and nulls on a PS basis, and reconsidered the emission geometry of its MP and IP. §2 describes the observations, §3 details aspects of our analyses, §4 builds a geometrical model, and §5 presents our thorough null analysis. §6 then provides a summary and discussion of our results.

Table 1. Observations

Band	MJD	BW (MHz)	Resolution (°)	Pulses (#)
P band	53966	25	0.31	7038
L band	54540	300	0.21	5470

2 OBSERVATIONS

The observations used in our analysis were made using the 305-m Arecibo Telescope in Puerto Rico. The 327-MHz (P band) and 1400-MHz (L band) polarized PSs were acquired using the upgraded instrument together with the Wideband Arecibo Pulsar Processor (WAPP[1]) on 2006 August 19 and 2008 March 15, consisting of 7038 and 5470 pulses, respectively. The auto- and cross-correlations of the channel voltages were three-level sampled and produced by receivers connected to linearly polarized feeds at L band and circularly polarized feeds at P band. Upon Fourier transforming, sufficient channels were synthesized across a 25- MHz (100-MHz at L band) bandpass, providing resolutions of approximately 1 milliperiod of longitude. The Stokes parameters have been corrected for dispersion, interstellar Faraday rotation, and various instrumental polarization effects. At L band, four 100-MHz channels were observed with centers at 1170, 1420, 1520, and 1620 MHz. Both of the observations encountered virtually no interference (hereafter RFI), except for the 1620 MHz channel at L band which was disregarded. At L band, the lower three 100-MHz bands were appropriately delayed and added together to give a 300-MHz effective bandwidth. The PPAs of the two observations are approximately absolute in that they have been corrected for both ionospheric and interstellar Faraday rotation.

3 ANALYSES

Figure 1 presents the polarized profiles and polarization-angle (hereafter PPA) histograms of pulsar B1944+17 at both 327 and 1400 MHz. While these profiles are familiar, it is useful to inspect them in detail. Notice that the half-power or equivalent width of the star's roughly symmetrical profile increases greatly at higher frequencies; whereas the ±20°-longitude interval over which significant emission is observed changes hardly at all. The PPAs also reiterate this circumstance clearly; the discontinuous "orthogonal" polarization mode (hereafter OPM) extends over the full ∼40° width of the profiles, whereas the more prominent OPM occupies a more restricted longitude range at the lower frequency. As the PPAs are nearly absolute and the two OPMs lie conveniently in the upper and lower halves of the PPA panel, we will refer to them as the "positive" and "negative" polarization mode, respectively.[2] The star's profile has been classified previously (R93) as belonging to the conal triple (c**T**) class; looking more closely, however, at the overall L-band form, it would be more accurate to regard it as exhibiting a hybrid c**T** and conal quadruple (c**Q**) behaviour. This said, the two profiles are so different in form that it is not easy to see how to align them. Rather, we have used the structures of stationary modulation on the leading and trailing edges of the PSs, and we note that this tends to align the profile edges but not the peaks. We will come back to considering how these characteristics should be interpreted below.

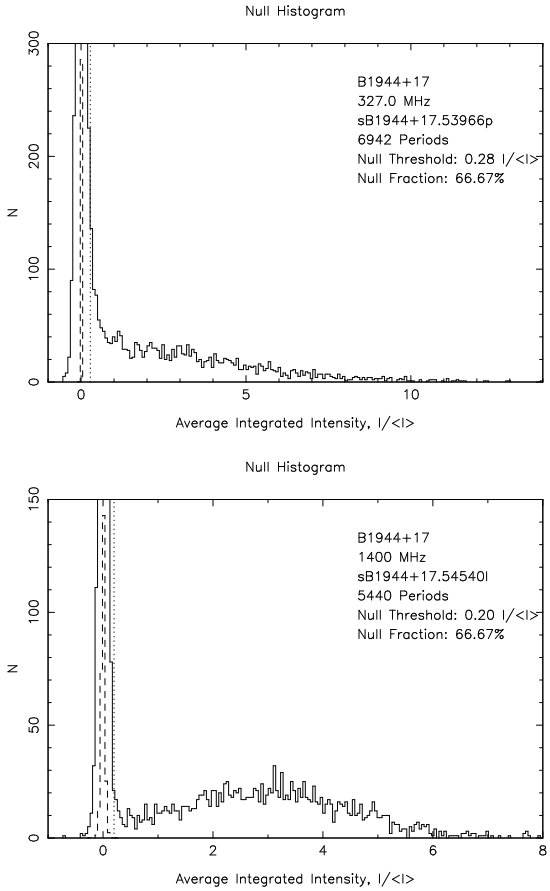

Figure 2. Null histograms for B1944+17 at P (top) and L (bottom) bands, respectively. The histogram peaks (at 1110 and 980) corresponding to the large null fractions have been truncated in order to better show the pulse-amplitude distribution. Despite the high S/N, the star's null- and pulse-energy distributions overlap, so that the nulls and pulses cannot be fully distinguished, though this difficulty is more severe at P band than at L band. Plausible, conservative thresholds (shown by dotted vertical lines) of 0.28 and 0.20 $<I>$, respectively, indicate that 2/3 of the pulses are nulls or pseudonulls.

[1] http://www.naic.edu/~wapp

[2] Interestingly, Hobbs *et al.*'s (2005) determination of B1944+17's proper-motion direction of 174°±29° gives the possibility that the fiducial PPA is aligned with the star's velocity vector in the sense of Johnston *et al.* (2006) and Rankin (2007). Of course, even if so the double ambiguity of supernova "kick" orientation and OPM identification make interpretation impossible at this time.

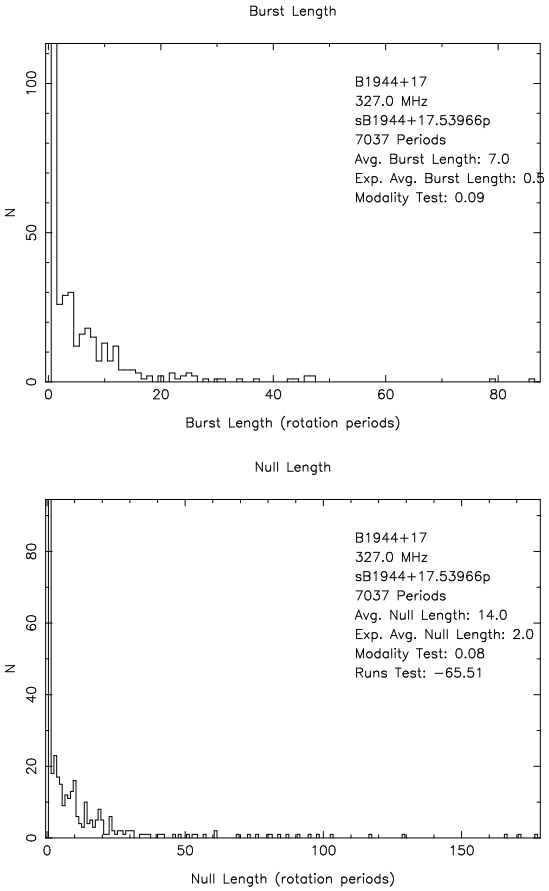

Figure 3. Burst- and null-length histograms corresponding to the P-band observation and threshold in Figure 2. These distributions show unsurprisingly that burst and null lengths of a single period are highly favored; however, we also see that bursts can last up to approximately 90 P_1 and nulls up to about twice this! Thus, in the language of the Runs Test, the nulls occur non-randomly in the PS by virtue of being "undermixed" (see text).

3.1 Non-Random Null Distribution

In our observations, B1944+17 nulls about 2/3 of the time, somewhat higher that the 60% value given by DCHR. The majority of these null pulses can readily be distinguished from the bursts; however, there is a small proportion of weak pulses that are difficult to identify as either nulls and pulses. Interestingly, the distinction between nulls and pulses is easier to define at L band, as can be seen in the respective null histograms of Fig. 2.

Given that the nulls and pulses cannot be fully distinguished, we can choose an intensity threshold that will be conservative and reliable either in selecting pulses or nulls, but not both. In Fig. 2, we have taken the latter option—that is, using low thresholds that will tend to slightly underestimate the null population. Then, using this conservative discriminator of nulls, we have computed the burst- and null-length histrograms in Figure 3. These show that 1-pulse bursts and nulls have the highest frequency, but we see that very long bursts and nulls also occur. In this 7000-pulse observation, a few bursts of 40-50 and a couple of 80-90 P_1 were encountered as well as frequent long nulls ranging up to 175 P_1. So even qualitatively we see immediately that the nulls in B1944+17 are distributed within the PS in a very non-random manner.

Recent investigations into pulsar nulling have raised two important new questions about their distributions: a) whether they are randomly distributed (*e.g.*, Redman & Rankin 2009; Rankin & Wright 2007); and b) whether they are periodic (HR07/09). The tendency of B1944+17's bursts and nulls to clump into "runs" of roughly some 20-100 pulses immediately indicates a non-random distribution (as with such a large null fraction, one would expect to see few long "runs" in any given observation). Application of the above RUNS test to our observations gives values $\lesssim$–60, verifing this conclusion, as any value $\leqslant$1.96 is indicative of a non-random "undermixing". Regarding null periodicity, we find only a suggestion in our observations of a very long periodicity—far too long in relation to their total length for us to be certain.

Thus the bursts and nulls of B1944+17 can be regarded as falling into two categories: a) short bursts or nulls of 1-15 P_1 that show a roughly random distribution, and b) medium to long bursts or nulls (>20 P_1) that can occasionally persist for several hundred pulses and are patently non-random.

3.2 Modes of emission

We here investigate the properties of the four modes identified by DCHR. Following their convention, we refer to the three drift modes as A-C, and the final burst mode as "D". The defining characteristics of modes A-D are the same at both P and L band, as are their frequencies of occurrence.

The four modes can be readily distinguished by eye due to their unique subpulse structures and intensities, as shown in Figure 4. The transitions between modes occur on a time scale of less than one pulse—*i.e.*, there are typically no observable "transitions" between modes [3] We find that within a sequence of 10^3 pulses there is a high probability of finding at least one occurrence of each mode. It is interesting that this pulsar, which displays an almost overwhelming variety of behaviors, is quite reliable in how often it does so.

As seen in the colour polarization display of Fig. 4, the star's mode changes are usually punctuated by nulls, though there are some combinations of mode changes that characteristically occur adjacent to one another.

3.2.1 Modal distinctions in subpulse structure

As modes A and B exhibit subpulse drifting, they can best be characterized by their P_2 and P_3 values, where P_2 is defined as the separation of subpulses within a period, and P_3 is the separation between drift bands at a fixed pulse phase. Mode C characteristically displays an organized yet stationary subpulse structure. Lastly, we classify those pulses which show no organized subpulse structure as mode D; it is worth noting that mode D is significantly weaker than the others.

Table 2 gives P_2 and P_3 values for modes A, B, and C. The A mode is characterized by prominent intervals of remarkably precise drifting subpulses–which is paradoxical

[3] With two notable exceptions, discussed in the null section.

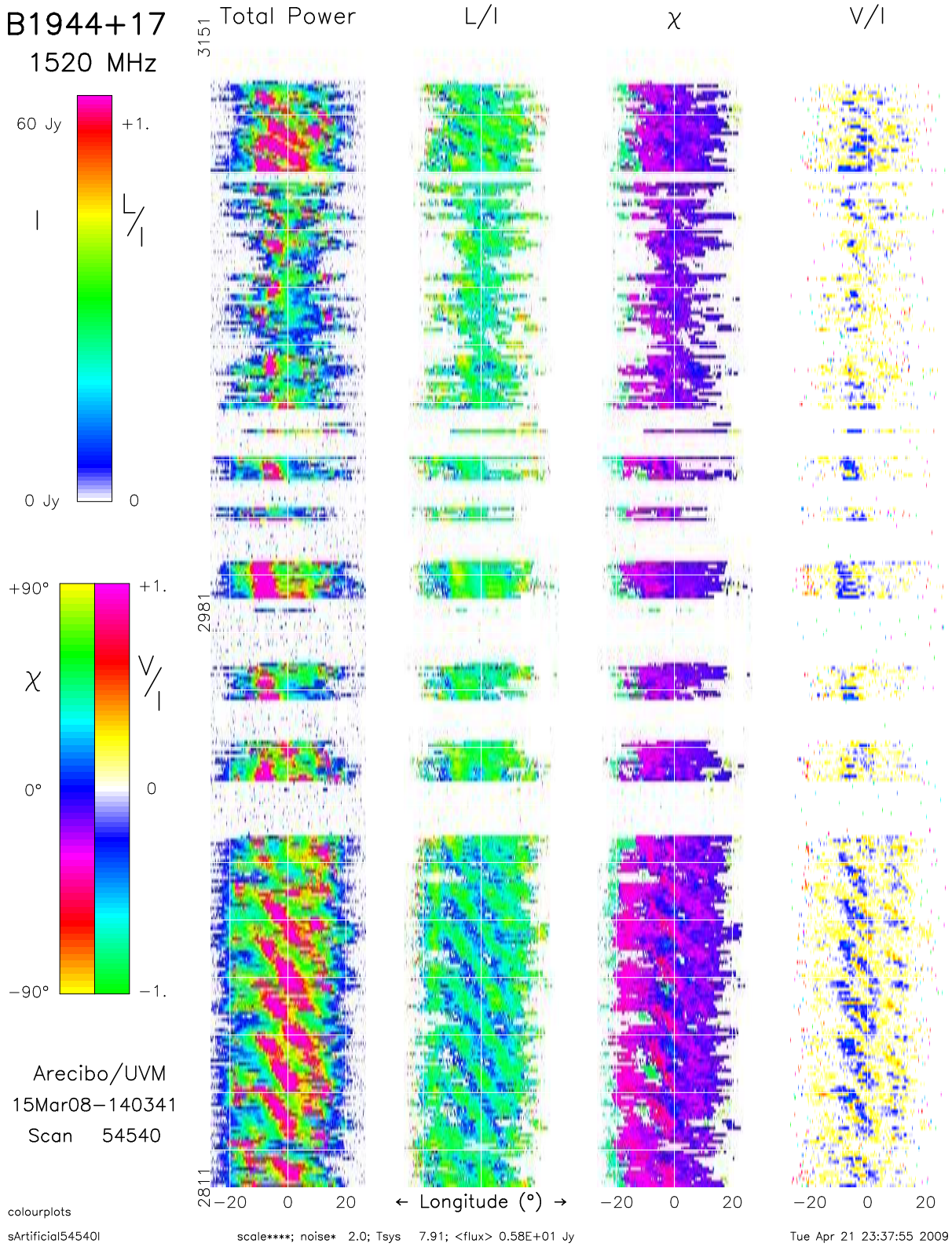

Figure 4. Artificially ordered pulse-sequence polarization display showing several of the pulsar's PS behaviors. The bright and ordered subpulses of mode A begin around pulse 2811 and last for 110 periods. Mode A is succeeded by a null and then mode C. Mode C is characterized by roughly stationary subpulses and a quasi-periodic cycle of short bursts and nulls. The next 200 pulses (4450-4600) are mode D, the weakest and least structured of the star's modes. Note the weak evidence of subpulse structure. Mode D is succeeded by a bright and very well defined mode B; the two modes are separated by a three-period null. The total power I, fractional linear L/I, PPA χ, and fractional circular polarization V/I are colour-coded in each of four columns according to their respective scales at the left of the diagram. Both the background noise level and interference level of this observation is exceptionally low with the latter effectively disappearing into the lowest intensity white portion of the I color scale.

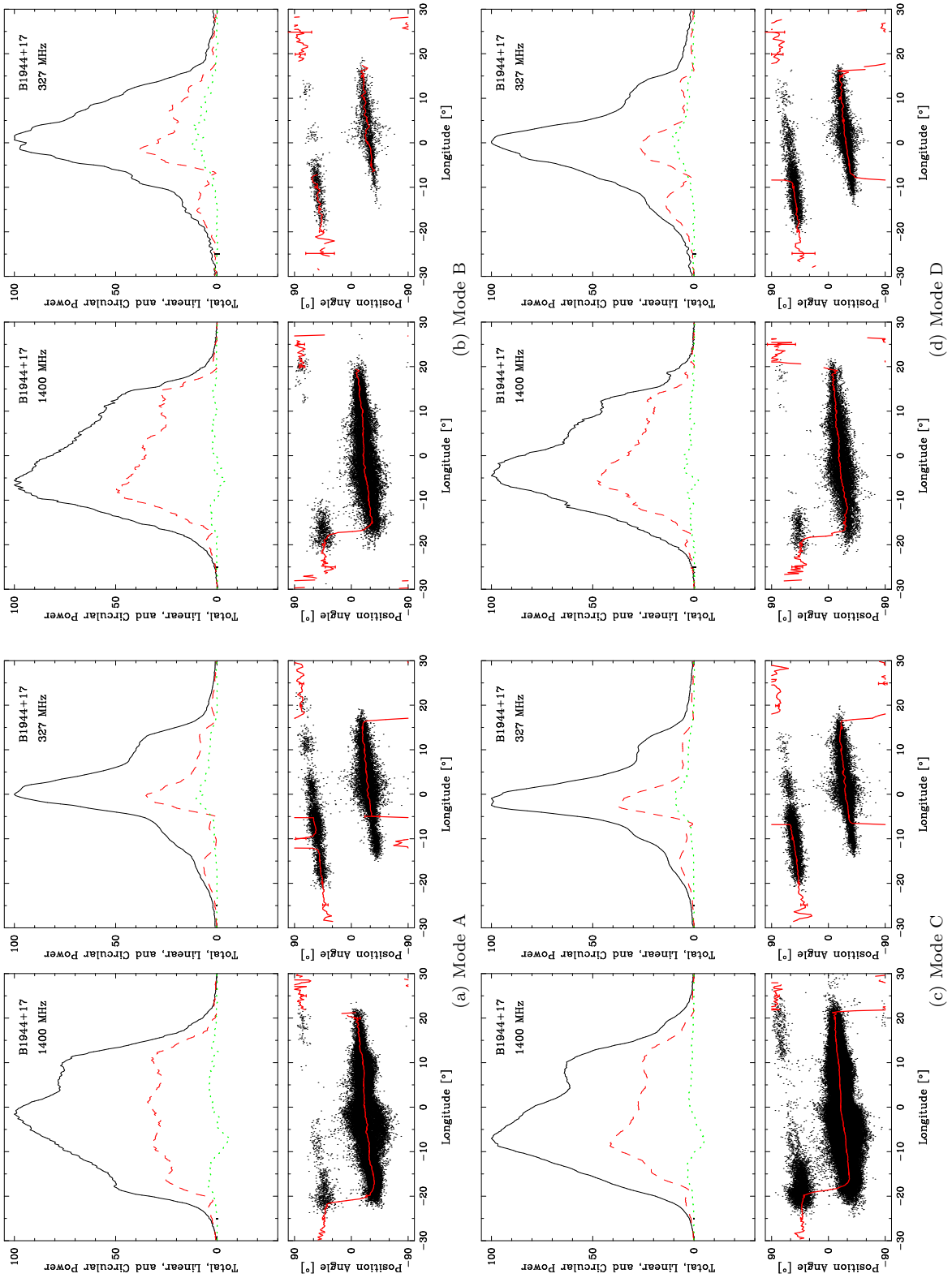

Figure 5. Partial polarized profiles after Fig. 1 for the four modes at L and P band. The base width within which there is measurable emission is constant in all the modes at both frequencies. There is, however, significant variation in the FWHMs of the various modes at the two different bands. Most notable is the narrowing of the FWHM at P band, clearly displayed in every mode. Also, at L band the FWHMs of modes A and C are broader than those of modes B and D. Conversely, at P band the FWHMs of modes B and D are broader than those of modes A and C. Numerical values for modal properties are summarized in Table 2.

Table 2. Emission Modes of B1944+17

Mode	Frequency Band	P_2 (°)	P_3 (P_1)	Percentage of total pulses	Number of Bursts	Number of Drift Bands	Average Burst Length	FWHM
A	L band	12.2±1.0	13.9 ± 0.6	8.4±0.05	14	25	32.5	29
	P band	13.5±1.0	13.5 ± 1.1	6.4±0.05	11	33	41.1	10
B	L band	11.0±1.6	6.5 ± 1.7	3.3±0.05	8	9	22.0	26
	P band	8.5±1.7	5.6 ± 1.8	1.4±0.05	8	10	11.9	18
C	L band	12.1±1.1	n/a	17.9±0.05	118	n/a	8.1	28
	P band	13.6±0.9	n/a	8.8±0.05	78	n/a	8.0	9
D	L band	n/a	n/a	4.4±0.05	22	n/a	11.0	21
	P band	n/a	n/a	20.6±0.05	119	n/a	12.1	12

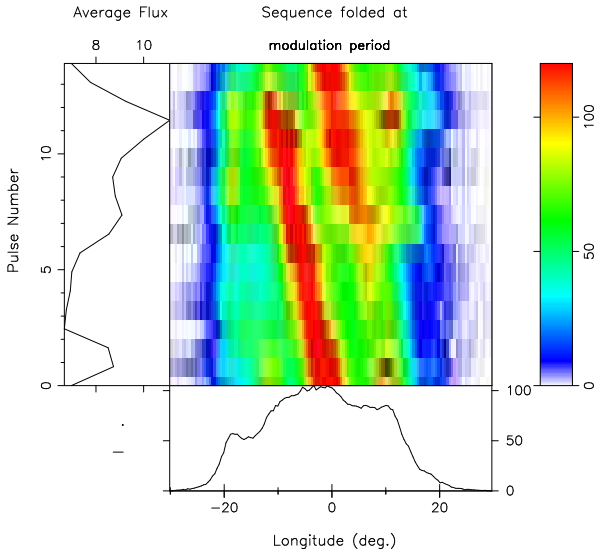

Figure 6. A 50-P_1 mode-A interval at L band. The PS has been folded at a P_3 of 14 $P-1$. The fold length was chosen to demonstrate that the conal outriders, seen at the leading edge of the pulse window, fluctuate with a period equal to mode A's P_3.

considering the star's otherwise unpredictable and discontinuous behavior. Mode A is unique in its regularity and is marked by its negatively-drifting bands with a roughly 14-P_1 P_3. Two bright, central subpulses are usually seen in mode A.

At L band, weak subpulses on the outer edges of the profile turn on and off with a period that is comparable to mode A's P_3; see Figure 6. Mode A always appears in bursts having durations of more than 15 periods; however, usually these bursts are even longer, typically some 60 – 100 P_1—and, remarkably, these A-mode intervals are very rarely interrupted by nulls.

The drifting subpulses of mode B are visibly less ordered than those of mode A; however they are clearly structured and negatively-drifting. P_3 is approximately half that of mode A at both L and P band, however due to its irregularities these values cannot be measured with the same degree of precision as they can be for mode A. The B mode characteristically lasts for less than 25 P_1.

The third drift mode, C, displays three roughly stationary subpulse drift bands ($P_3/P_2 \approx 0$), with the components' relative intensities being variable. Mode C manifests itself in a complex variety of ways: most often the three components are of an intensity approximately equal to one another; see Fig. 4. However, one or two of the components intermittently either turns off or notably weakens relative to the other two; every combination of the three constituent components was observed. The P_2 value for mode C is similar to that of mode A, taking into account the presence or absence of its three constituent features.

It is possible that the nearly vertical drift bands in mode C result from a near stoppage of carousel rotation. Because of the other similarities between modes A and C, it is likely that this "stopping" happens during what is otherwise known as mode A. The difference between modes A and C is therefore only the carousel motion, not the fundamental subpulse structure. This dynamic accounts for the varying number of subpulses observed in mode C. In mode A, as the subpulses drift across the pulse window, anywhere between 1 and 3 may be seen depending on the modulation phase—*i.e.*, see Fig. 6.

In mode C short bursts and nulls alternate quasiperiodically with each burst or null lasting some 10 P_1 or so, and switching back and forth up to 10 times. The length of these segments is very comparable to the P_3 of mode A.

Deich *et al.* first referred to mode D as "chaotic"—that is, displaying little perceptible order in its subpulses. Our investigation has uncovered a slightly different story for mode D. The mode-D emission does not usually span the entire pulse window, see Fig. 4. While its sparse subpulses are overshadowed by the bright and ordered ones of modes A, B and C, they appear to have an underlying characteristic structure. Mode D's brightest subpulses appear approximately every 5–10 P_1 on the leading edge of its substantially narrower emission window. This withdrawal of emission in the profile wings is unique to mode D..

3.2.2 Modal distinctions in total and linear power distributions

Figure 5 gives partial polarized profiles for each of the four modes at L and P band. The profiles have different total power and total linear forms in the different modes. Most evident are their different modal widths in each of the bands.

Mode A has the broadest modal profiles; see Figure 5(a). The L-band profile displays a nearly uniform distribution of linear power across the pulse window, showing only small dips that correspond to the subpulse separation. Its

leading edge is marked by a distinct shoulder at both L and P band, also visible in the linear power, a feature hardly seen in any of the other modes at L band. The bright central subpulses in mode A display a linear power distribution that indicates there are in fact two distinct features that lead the central peak. They can be identified at both bands, though the second one is weaker at P band, nevertheless distinguishing itself as a unique feature. Also in both bands, the trailing subpulse features are brighter and more clearly defined than the leading ones.

The mode-B profiles display a slightly narrower FWHM in than mode A; see Table 2 and Fig. 2. The leading feature in mode A's profile is clearly visible in mode B at P band but is very weak at L band; see Figure 5(b). At L band, the central peak of mode B occurs ∼6° earlier than in mode A; at P band the peaks of the two modes occur in the same location. The trailing feature in mode B is poorly defined, however this is likely due to the dense drift bands blurring the intensity distribution between the leading and trailing features, rather than a decrease of subpulse intensity.

Mode C displays a FWHM width nearly as broad as that of mode A; see Table 2. There is more evidence for the leading feature in the linear power distribution of mode C than in mode B. As in mode B, the central peak in mode C at L band is shifted 6° earlier relative to the peak in mode A, whereas at P band they occur at the same longitude. The trailing component is very well defined in mode C in the profiles of both bands.

Mode D displays a significantly narrower profile at L band compared to the other modes. As in mode B, the leading component is very poorly defined at L band, though there is some evidence for it in the linear power distribution. At L band, the central peak of mode D is shifted approximately 4° compared to that of mode A. At L band, the trailing feature is slightly more distinct in mode D than in mode B, though it remains weak. The trailing feature at P band is well defined.

3.2.3 Mode changes

Mode changes are often punctuated by nulls, with two distinct exceptions: First, a small portion of mode changes are characteristically not interrupted by a null. We find that mode D often precedes modes A and B and sometimes succeeds mode B continuously. Second, nulls do not necessarily result in mode changes. Mode C (discussed below) characteristically displays a pattern in which the emission turns on and off in segments of short 10-15 P_1 bursts and nulls. Short nulls are associated both with this mode-C emission pattern as well as with other less notable mode changes.

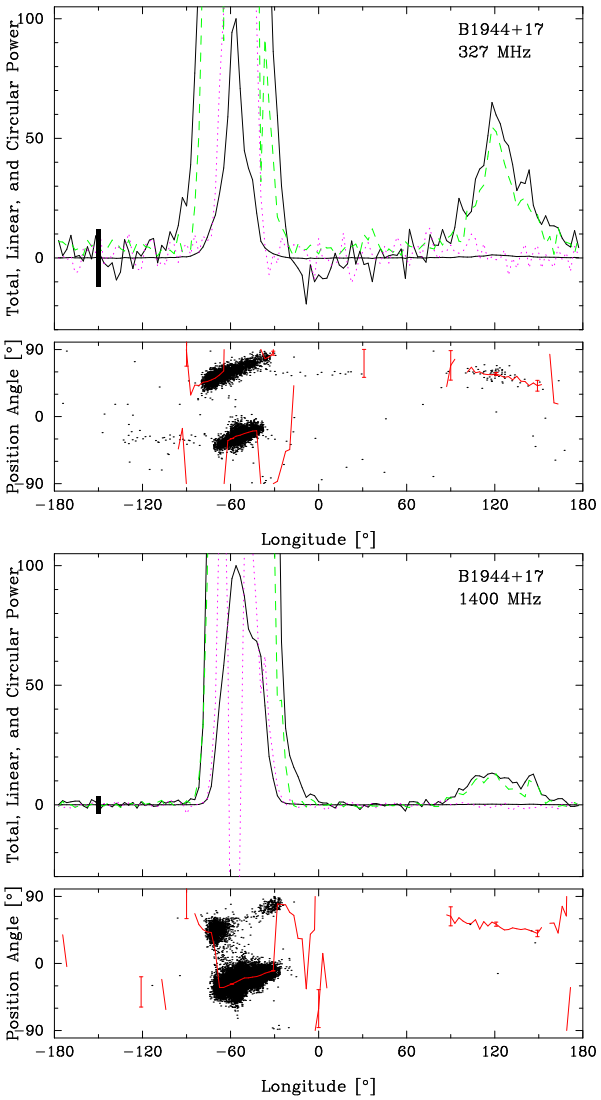

Figure 7. Full period polarization profiles (after Fig. 1) of the P- (upper) and L-band (lower) partial PSs containing the pulses (falling above the thresholds in Fig. 2), not the nulls (2403 and 1803 pulses, respectively). Here, the total power is shown at full scale and then Stokes I, L and V are replotted at 50X scale in order to reveal the structure of the interpulse; otherwise the displays are identical to those in Fig. 1. Only 128 longitude bins were used across the full profile so as to maximize the S/N of each sample. Note the virtually complete IP linear polarization and the similarity in half-power widths between the IPs in the two bands. Note also that the centers of the PPA traverses of the IP and MP (positive OPMs) both fall at about +60° and have opposite slopes.

3.3 Main Pulse – Interpulse Relationship

We have also used the conservative thresholds of 0.28 and $0.20 < I >$ to build partial P- and L-band PSs of the pulses and nulls. Full period polarization profiles corresponding to the pulses (not the nulls) are shown in Figure 7 and are similar to the MP profiles in Fig. 1 except that Stokes I, L and V are replotted at 50X scale to reveal the structure of the IP. Here we see clearly for the first time that the B1944+17 IP is fully linearly polarized (and has negligible circular), that its half-power width is very comparable at the two frequencies, and that its IP traverse is centered at virtually the same PPA as the MP positive-mode, but with a negative slope. In the 327-MHz profile, the discrete PPA dots under the IP profile show that some IP samples are strong enough to define their linear polarization; thus the IP is not uniformly weak, but exhibits a range of intensities. We can also confirm that the IP-to-MP intensity ratio (S_{IP}/S_{MP}) decreases with frequency, being about 1% at P and some 0.2% at L band. HF86 reported values of about

3% at 430 MHz and 0.3% at L band. Notably, they found that most pulsars with IPs show a similar decrease as frequency increases. More perplexing was HF86's finding that the MP-to-IP spacing ($\Delta\phi_{IP-MP}$) decreases by some 10° between P and L band, and given the drastic changes in MP form it is not fully clear how such a change could even be consistently measured.[4]

Using such partial PSs for the pulses (but now at both the restricted and full longitude resolutions), we also computed correlation functions that included the longitude ranges of both the MP and IP. These showed no significant (>3 standard deviations in the off-pulse noise) level of correlation at lags of either 0 or ±1 pulse.

We also computed partial profiles for the null partial PSs, having lengths of 4635 and 3667 at P and L band, respectively. In these, we were able to find neither significant total power nor any correlated PPAs that might indicate weak linear polarization in the baseline regions. This circumstance argues very strongly that the IP either nulls, or remains very inactive, during MP nulls.

4 EMISSION GEOMETRY OF THE MAIN PULSE AND INTERPULSE

At various stages of our analyses we had indications that the baseline regions of the full period profiles were significantly linearly polarized. In order to explore this further, we reprocessed our observations in a manner such that no baseline level was subtracted from Stokes Q and U. We then found a significant level of linear polarization in both regions between the MP and IP corresponding to some 0.25% of MP peak at P and 0.8% at L band. In both cases the PPAs associated with this baseline linear polarization are nearly flat, suggesting that only one Stokes parameter is well defined, therefore we have concluded that this polarization cannot be well measured with our polarimeter configurations.[5] Again, we stress that this baseline linear power is associated with the pulses and not the nulls! HF86 also allude to a "bridge" of total power emission between the star's MP and IP (see their fig. 2d and the associated discussion).

Regardless of whether the star is classified as a member of the c**T** or c**Q** class, it can be said with confidence that our sightline crosses two concentric emission cones. The weaker cone is encountered on the profile edges and exhibits similar properties and dimensions at the two frequencies. It is the stronger central emission that shows a "resolved double" pattern above 1 GHz and a more "single" form at meter wavelengths. Two aspects of this profile's evolution are quite unusual (*e.g.*, R93): a) that the central emission pattern narrows (shows a smaller equivalent width) at lower frequencies, and b) that the "outriding" component pair retain essentially the same dimensions between the two bands. Generally, we encounter outer cones on profile edges, and these show substantial "spreading" with wavelength; whereas inner cones are seen inside the outer ones and show little spectral variation in their dimensions. In B1944+17 these usual expectations seem reversed; how could this occur?

4.1 Assembling the Relevant Evidence

Careful reference to the total power profiles of Fig. 7 shows that the MP and IP are both rather broad—as is expected for a small value of α—with emission extending over most or all of 60° in each case. Moreover, HF86 notwithstanding, the MP to IP spacing is close to half the rotation period. Given the complex and changing form of the MP in particular, it is difficult to be more precise than this.

Several aspects of the linear polarization are also important to note: First, the absolute PPAs associated with the central longitudes of the MP and IP are nearly identical, arguing that the respective emission regions are either conjunct or in opposition along a given magnetic longitude. Second, the PPA traverses under the MP and IP have opposite senses, indicating that magnetic longitude is increasing for one and decreasing for the other. At both frequencies, 90° OPM-dominance jumps occur on both the leading and trailing edges of the profiles.

Third (see Fig. 1), the MP PPA traverse is unusually shallow. Its sweep rate R ($= \Delta\chi/\Delta\phi$) is only some $+0.8°/°$ and remarkably linear across the bodies of both the P and L-band profiles. The shallow PPA traverse indicates that the magnetic colatitude α and sightline-impact angle β are similar and both small (*i.e.*, the sweep rate $|R|=\sin\alpha/\sin\beta$). Interestingly, the negative sweep rate of the IP has a very similar slope. At both frequencies, 90° OPM-dominance jumps occur on both the leading and trailing edges of the profiles.

Finally, the interpulse emission is of an entirely different character than that of the MP. The MP has a complex structure of regions with different dynamics and OPM activity, whereas the IP is more nearly unimodal in form (though with low persistent peaks) and fully linearly polarized. In contrast to the MP, it displays a continuous, smooth PPA traverse—*i.e.*, it does not show any "90° jumps" as the MP does. These MP and IP properties provide crucial information about the emission geometry as we will see below.

4.2 Building A Geometrical Model

While B1944+17's IP has been known for more than 20 years (HF86), its polarization properties are measured here for the first time. Therefore, all previous efforts to understand the star's basic geometry have been based on its MP properties alone. HF86 speculated about whether the IP reflected a single or two-pole configuration, but made no attempt at a quantitative model. The star's unusually shallow R value presents a major difficulty for any model. Indeed, the only published model (R93) views the pulsar's MP profile as c**T** and obtains reasonable dimensions for the inner and outer cone—but only by assuming that the apparent R value was somehow too flat. Taking R as $+3°/°$ (more than three times

[4] Thanks to Tim Hankins, we have been able to examine the interpulse-discovery observations that were reported in HF86, and we can see how their interpretation of a frequency-dependent $\Delta\phi_{IP-MP}$ arose. At that time, it could not have been realized that the unusual shape changes of B1944+17's MP make it nearly impossible to correctly align profiles of different frequencies.

[5] The L-band system consists of dual linears and the P band dual linears with a circular hybrid between the feed and the cal injection; thus in neither system are Stokes parameters Q and U determined fully by correlation of the receiver voltages.

the actual value), she obtained α and β estimates of some 19° and 6.1°, respectively. As R93's β estimate is better determined by virtue of the necessity that the sightline traverses through emission cones of typically 10° dimensions, the actual sweep rate of $+0.8°/°$ implies that α will be even smaller than $|\beta|$. Finally, this also suggests strongly that the observer's sightline to B1944+17 largely remains inside its emission cones!

The half- or eqivalent widths of the MP and IP are roughly equal and occupy opposing ∼45° or 1/8 sections of the star's rotation cycle. Moreover, the similar PPA ranges and opposite slopes of the MP and IP traverses argue that our sightline cuts these regions within the same range of magnetic longitude but at different colatitudes. This symmetry is consistent both with an orthogonal rotator model (in which the MP and IP emission comes from the two respective poles) as well as a single pole model (wherein both MP and IP are emitted within a single polar region). Notably, the extreme shallowness of the sweep rate R is more consistent with the latter configuration.

The very small α and β values indicate that the pulsar is a nearly aligned rotator with the Earth positioned almost directly above its "nearer" polar cap of emission. According to this model, the MP is a result of our sightline first crossing the inner cone of emission obliquely, then making a tangential cut through the outer cone, and finally recrossing the inner cone symmetrically. Such an "inside out" sightline traverse accounts for the stability of the outer parts of the MP profile as well as the unusual frequency dependence of the middle region. Moreover, the weak IP feature can apparently be understood as a grazing encounter of the sightline with the core beam—such that the MP and IP are centered on the same field lines that are cut in opposite directions.

Finally, we can assemble the elements of a quantitative model for the emission geometry of B1944+17. Following R93 we know that the outer and inner conal beams have particular dimensions at 1 GHz, here specified in terms of the outside half-power points (which for a 440-ms pulsar) are 8.7° ($=5.75°P_1^{-1/2}$) and 6.5° ($=4.33°P_1^{-1/2}$), respectively. A similar model is available for the peaks of conal beams (Gil *et al.* 1993) such that these fall at 6.9° ($=4.6°P_1^{-1/2}$) and 5.6° ($=3.7°P_1^{-1/2}$). No such study has determined the inner half-power dimensions of conal beams, but if we assume that they are radially symmetric, we can estimate their inner dimensions from the above data. These values are then 5.2° ($=3.45°P_1^{-1/2}$) and 4.5° ($=2.97°P_1^{-1/2}$) as above, respectively. These conal beam characteristics are illustrated in Figure 8: the outer and inner cones are hashed in blue and green, respectively, up to their half-power levels, and their peaks are indicated by heavy colored dashed lines. Note that the two beams overlap significantly (as they do in actual profiles) and this overlap region is hashed in cyan. Finally, the core beam is shown in red hashing centered on the magnetic axis ("M") out to its 1.8° ($=2.45/2P_1^{1/2}$) half-power point.

In the above radiation-beam context, what is the trajectory of our sightline to B1944+17? As mentioned above we can suppose that its maximum and minimum extensions touch the outer conal beam and core, respectively. Necessarily it will cross these emission regions obliquely, with most of its motion in magnetic longitude, so that the PPA slope will be maximal and roughly linear under the MP and IP.

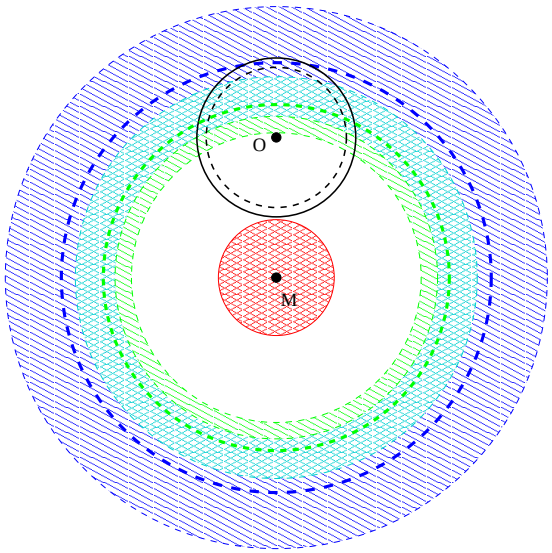

Figure 8. Diagram showing the apparent sightline geometry of pulsar B1944+17. The outer cone is shown in blue, the inner cone in green, and their overlap region in cyan. The core beam is then shown in red. The radial peaks of the respective cones is shown by thick blue and green dashed lines. The edges of the beams show their half power points (see text). The magnetic axis is marked with an "M" and the rotation axis with an "O". As we know little for B1944+17 about the frequency dependence of the beam dimensions, we have used their (R93) nominal 1-GHz values—e.g., 8.7° for the outer beam's outer 3-db radius (see text). The observer's sightline orbit then makes a small circle around the rotation axis such that it touches both cones and the core beam. The beam pattern has a larger angular size at the lower frequency, so we show the *relative* size of the sightline orbit within the beam pattern. The P and L-band sightlines are then indicated by dashed and solid black lines, respectively.

Were sine waves fitted to the PPA traverses in Fig. 7 (surely not the correct function, but an adequate approximation), one can readily see that its total PPA amplitude would be roughly 50-60°—which also represents the total PPA excursion in magnetic longitude. Or, said differently, the sightline circle [centered on the rotational pole "O" in the diagram] must have an angular radius that is comparable to the angular displacement of its center from the magnetic axis. This, of course, is just the condition that $\alpha \approx \beta$ which follows from the shallow PPA sweep rate R.

The respective L (solid) and P (dashed) sightline trajectories are then indicated in Fig. 8 as heavy black circles centered on the rotation axis. Of course, the actual angular radius of the sightline circle is constant. Given, however, that the B1944+17 profiles provide very little information about the "conal speading" at meter wavelengths, we have chosen to illustrate the pulsar's geometry using the well determined 1-GHz dimensions of the beam structure. In relative terms, then the sightline at L band extends just past the radial maximum point of the outer cone, such that it exhibits a c**Q** structure; whereas the P-band traverse falls short of this point and has a c**T** form. In both cases the sightline encounters the core producing the IP.

The multiple lines of evidence that our analyses of this pulsar provide point strongly to the unusual emission geometry discussed above. Were reliable baseline polarimetry

available, the sightline traverse could be modeled in considerable detail and the actual dimensions of the several beams estimated through fitting. Unfortunately, this work remains beyond the scope of this paper. Nonetheless, we believe that the circumstances responsible for the B1944+17 interpulse are largely understood—that both the MP and IP are emitted by a single pole and that the IP is very likely weak core emission.

5 HOW CAN WE UNDERSTAND B1944+17'S NULLS?

Pulsar B1944+17 has been most famous for its remarkably long null intervals, which contrast so beautifully with its intense and well organized burst sequences. The star is in the null state some 2/3 of the time, on average. Notably, this value is the same for both the main pulse and the interpulse.

Since Backer's first documentation of pulsar nulling in 1970, the principal question surrounding nulls has been one of causality. Here we discuss and distinguish between nulls that are likely caused by two entirely different mechanisms: empty sightline traverses across a rotating carousel, and cessations of emission. We find that the two null categories, empty sight line traverses and emission cessations, can be distinguished by their characteristic lengths, and we will therefore refer to them as such: the former being short nulls, and the latter the long ones.

5.1 Null Analysis

It is important to note that the distinction between short and long nulls is not a clear one. In this investigation, the numerical boundary was set as approximately the P_3 values —*i.e.*, long nulls last for more than one "sweep time". This delineation of a carousel "beamlet" is by no means exact; however we are more interested in the possibility that there are two different types of nulls B1944+17, than in defining their features precisely.

5.1.1 Short Nulls

Short nulls can be found in virtually any context of this star's emission—that is, they are not unique to a particular mode, nor do they only occur between mode changes. The short null average profile was artificially constructed by summing together all null pulses which belonged to nulls under 15 P_1 in length. The total power in the short null MP average profile was nonzero—*i.e.*, it did not represent noise, rather there was very clear indication of emission. See Figure 9. It is difficult yet of great importance to decipher whether this non-zero power is the result of emission from (a) consistent low intensity emission through out the null and/or (b) a small number of high-*er* intensity pulses that skew the average.

To reduce the probability that the non-zero intensity was due to (b), the few pulses for which there was visible power (*i.e.*, perhaps "should" have been called weak bursts) were removed by hand from the artificial PS. It was after this procedure that the short null profile was found to exhibit significant power, whereas the long null profile was indistinguishable from that of noise. We conclude that the power in the short nulls is due to (a): consistent low intensity emission not detectable on a single pulse basis.

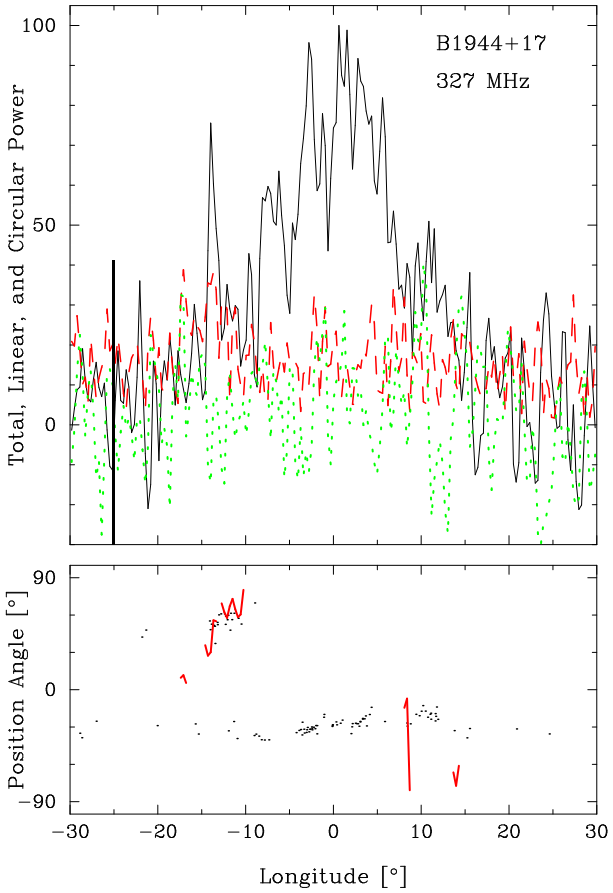

Figure 9. The short null profile —*i.e.*, the sum of all pulses which participate in nulls less than 15 periods in length. An intensity threshold of 0.28 $I/<I>$ was used to differentiate between nulls and bursts. Then, those pulses in the short null sequence which still displayed visible power (appeared to possibly be weak bursts) were removed by hand. The remaining non-zero power indicates that there is a weak intensity signal (not detectable on a single pulse basis) present in the pulses which participate in short nulls.

Short nulls are more or less randomly distributed throughout the pulse sequence both at L and P band. Recall that B1944+17's subpulses consistently repeat behaviors (evidenced by the star's well defined modes) though not with any periodicity. It is not surprising that the nulls complimenting such modes appear consistently, but in a random distribution (*i.e.*, are not periodic).

Mode changes are often, though not always, punctuated by short nulls. Modes A and D are often intercepted by short nulls of some 1 – 3 P_1. Of the four modes, mode D is most frequently punctuated by short nulls. That the short nulls are empty sightline traverses is very consistent with what we observe in mode D. Mode C characteristically alternates short quasiperiodic bursts and nulls of some 10 – 20 P_1. These transitions between nulls and bursts appear to entail no turnoff as no possible such "partial null" was ever observed in the pulse window. Their characteristic length falls roughly on the boundary where we distinguish between short and long nulls. We have found no means of testing whether

these mode-C nulls represent the longest pseudonulls or the shortest of the long null intervals.

5.1.2 Long Nulls

The rest of the story belongs to the long uninterrupted null sequences. In contrast to the short nulls, the total power in the long nulls is exactly that of off-pulse noise, indicating that there is truly no measurable power from the star during those nulls. This is the case at both L band and P band.

Deich *et al.* looked for, but did not observe, transitions from the null-to-burst or burst-to-null state, that occured as the star's emission cone swept through the Earth's direction—*i.e.*, the star's emission turning off or on in the middle of the pulse window. In our investigation we found two such possible transitions at L band, one of which was from the burst to null state, and the other the opposite. Both transitions occurred approximately halfway through the pulse window and were marked by a sharp decrease or increase in emission intensity. Both transitions occurred on the edges of long null intervals. If the pulsar does cease its emission, it does so on a time scale of less than one period, in contrast with a gradual decrease or increase in emission.

As mentioned earlier, B1944+17's nulls last up to 300 P_1 in our observations. These long null intervals appear frequently, consistently, and in a highly non- random manner. Considering the noise-like character, length, and non-random distribution of the long nulls, the probability that the long nulls represent empty sight-line traverses is extremely small. The evidence assembled through our investigation indicates that the long nulls likely reflect cessations of emission. This finding would be strengthened by detecting a measurable decrease in spin down rate during the nulls, as measured in B1931+24, however at present we found that the intervals are too short for this to be possible.

6 SUMMARY AND DISCUSSION

The four modes of B1944+17 are distinct and well defined. Both the total power and the FWHM as displayed in the modal average profiles show consistent behaviors *within* different modes. The brightest and most ordered of the star's four modes is mode A, which consistently displays three to four subpulses that drift with a P_3 value of 14 periods. Mode B drifts at a faster rate and displays a P_3 of approximately 6 periods. It also has three subpulses, though they are characteristically less ordered than those of mode A. Mode C displays between one and three subpulses of similar brightness and order to those of mode A, however displays zero subpulse drift. Mode C may be interpreted as representing a carousel of subpulses organized in the same way as in mode A, but which is stationary. Lastly, mode D is the weakest of the four modes. Though it lacks the ordered drift bands displayed in the other modes, we find that it is not chaotic, as it had been previously described by DCHR86. Its brightest subpulses are in the leading edge of the pulse window, appear consistently at the same phase, and remain active for some 5 periods or so. We were not able to identify B1944+17's carousel configuration.

B1944+17 presents several challenges in determining its geometry. Unlike most pulsars, the equivalent width decreases with increased frequency, while the full width of the profile is constant with changes in frequency. Furthermore, it has a PPA traverse that is nearly flat. The PPA traverse of the MP and IP are identical in magnitude and exactly opposite in sign. Polarization and total power measurements of the MP and IP indicate that B1944+17 has an unusual single pole geometry. That is, the IP emission occurs exactly in opposition to the MP and along the same field lines. After careful calculations, reference to the MP, IP, modal average profiles, and measurements of IP and MP nulling patterns, we conclude that our sight line lightly brushes the core emission (IP) followed by an oblique crossing of the inner cone, outer cone, inner cone (MP), see Fig. 8. We find that the MP and IP are separated by approximately 180° at both L and P bands. The rarity of this geometrical situation may explain some of the unexpected PPA traverses that we have measured, as well as the unusually narrow width of the profile at low frequency, relative to its higher frequency counterpart.

B1944+17 is in the null state nearly 70% of the time. That is, there is a 2/3 chance that any given pulse will be a null rather than a burst. With this consideration, it is interesting to find in B1944+17 bursts characteristically lasting up to 100 P_1 and nulls lasting up to 300 periods. As expected, one period nulls appear with the highest probability. We found that nulls up to 15 P_1 in length occur with a roughly random distribution, whereas nulls longer than this are obviously non- random. Based on this result, we decided to investigate whether there are other differences between the short and long nulls. Indeed, we found evidence indicating that there are actually two distinct mechanisms that result in B1944+17's null pulses. The short nulls, of less than 15 P_1, display an average profile with a small amount of power, see Fig. 9. We interpret such nulls as being caused by empty sightline traverses through a carousel beam system—*i.e.*, they are the pseudonulls that result from the mechanism discussed above. The long nulls, on the other hand, display a profile exactly resembling that of noise. We interpret the long nulls as evidence for a true cessation in pulsar emission—*i.e.*, caused by the same mechanism identified by Kramer *et al.* (2006). With B1944+17 nulling nearly 70% of the time, it is not entirely surprising that there are two factors contributing to this behavior. Fundamentally, these two mechanisms operate independently and it is not unexpected that they should both be observed in a single star. It will be interesting to see whether there are other stars whose nulling behavior might be better understood through the same lense that we now understand the behavior of B1944+17.

It is exciting to find such an interesting combination of phenomena in B1944+17: mode changing, nulling caused by emission turn offs, nulling caused by empty sightline traverses through a rotating carousel, and a 180° interpulse that is the result of core emission, as the star has nearly aligned magnetic and rotational axes. We have thoroughly documented each of these behaviors, and have put forth a basic geometrical model that begins to tie them all together. In the future we hope this empirical investigation of radio pulsar B1944+17 will aid theorists interested in understanding pulsar emission and how it may relate to primary phenomena such as mode changing, nulling, and interpulses.

ACKNOWLEDGMENTS

We are pleased to acknowledge Geoffrey Wright, Joeri van Leeuwen and Tim Hankins for their critical readings of the manuscript and Jeffrey Herfindal for assistance with aspects of the analysis. We also sincerely thank both Tim Hankins for providing us with the original interpulse discovery observations, and Joel Weisberg for the ionospheric Faraday rotation corrections. One of us (IMK) sincerely thanks the UVM College of Arts and Sciences for the APLE Summer Fellowship that permitted her to begin this work. The other (JMR) thanks the Anton Pannekoek Astronomical Institute of the University of Amsterdam for their generous hospitality and both Netherlands National Science Foundation and ASTRON for their Visitor Grants. Portions of this work were carried out with support from US National Science Foundation Grants AST 99-87654 and 08-07691. Arecibo Observatory is operated by Cornell University under contract to the US NSF. This work used the NASA ADS system.

REFERENCES

Backer, D. C. 1970 *Nature*, 228, 1297
Backer, D. C. 1973, *Ap.J.*, 182, 245
Bhat, N.D.R., Rao, A.P., & Gupta, Y., *Ap.J. Suppl.*, 121, 483
Bhat, N.D.R., Gupta, Y., Kramer, M., Karastergiou, A., Lyne, A.G., & Johnston, S. 2007, *A&A*, 462, 257
Deshpande, A.A. & Rankin, J.M. 1999, *Ap.J.*, 524, 1008
Deshpande, A.A., Rankin, J.M., 2001, *MNRAS*, 322, 438
Deich, W. T. S., Cordes, J.M., Hankins, T.H., & Rankin, J.M., 1986 *Ap.J.* 300, 540
Gil, J.A., Kijak, J., & Seiradakis, J.H. 1993, *A&A*, 272, 268
Gil, J., Melikidze, G., Zhang, B., 2006 *A&A*, 457, L5
Hankins, T. H. & Fowler, L. A. 1985, *Ap.J.*, 304, 256
Herfindal, J. L., & Rankin, J. M., 2007, *MNRAS*, 380, 430
Herfindal, J. L., & Rankin, J. M., 2009, *MNRAS*, 393, 1391
Hobbs, G., Lorimer, D. R., Lyne, A. G., & Kramer, M. 2005, *MNRAS*, 360, 974
Johnston, S., Hobbs, G., Vigeland, S., Kramer, M., Weisberg, J. M., & Lyne, A. G. 2006, *MNRAS*, 364, 1397
Kramer, M., Karastergiou, A., Gupta, Y., Johnston, S., Bhat, N.D.R., & Lyne, A.G. 2003, *A&A* 407, 655
Kramer, M., Lyne, A. G., OBrien, J. T., Jordan, C. A., & Lorimer, D. R. 2006, Science, 312, 549
Lyne, A.G., & Manchester, R.N. 1988, M.N.R.A.S., 234, 477
Nowakowski, L., 1996, *Ap.J.* 457, 868
Pilkington, J.D.H., Hewish, A., Bell, S. J. & Cole, T. W., 1968, *Nature*, 218, 126
Rankin, J.M., 1986, *Ap.J.*, 301, 901
Rankin, J.M., 1993a, *Ap.J.*, 405, 285
Rankin, J.M., 1993b, *Ap.J. Suppl.*, 85, 145
Rankin, J.M., 2007, *Ap.J.*, 664, 443
Rankin, J. M. & Wright, G.A.E. 2007, *MNRAS*, 379, 507
Rankin, J. M. & Wright, G.A.E. 2008, *MNRAS*, 385, 1923
Redman, S. R., Wright, G.A.E., & Rankin, J. M., 2005, *MNRAS*, 357, 859
Redman, S. R., & Rankin, J. M., 2009, *MNRAS*, 395, 1529
Suleymanova, S. A., & Rankin, J. M. & 2009, *MNRAS*, 396, 870
Taylor, J. H., Huguenin, G. R. 1971, *Ap.J.*, 167, 273
Taylor, J. H., Manchester, R. N., Huguenin, G. R. 1975, *Ap.J.*, 195, 513
Wang, N., Manchester, R. N., & Johnston, S. 2007, *MNRAS*, 337, 1383 (astro-ph/0703241)
Weltevrede, P., Edwards, R. T., & Stappers, B. W. 2006, *A&A*, 445, 243
Weltevrede, P., Stappers, B. W., & Edwards, R. T. 2007, *A&A*, 469, 607